Available online at www.sciencedirect.com

ScienceDirect

Procedia Structural Integrity 11 (2018) 226–233

Structural Integrity Procedia

www.elsevier.com/locate/procedia

XIV International Conference on Building Pathology and Constructions Repair – CINPAR 2018

Effects of nonlinear modelling of the base-isolation system on the seismic analysis of r.c. buildings

Fabio Mazza[a,]*, Rodolfo Labernarda[a]

[a]*Department of Civil Engineering, Università della Calabria, 87036 Rende (Cosenza), Italy*

Abstract

Long-duration and high-amplitude horizontal velocity pulses are expected at sites located near an active fault; these are able to generate notable displacement at the level of the isolation system and pounding effects between closely spaced structural parts (e.g. in the case of an insufficient seismic gap between the elevator and building). A base-isolated commercial building, recently built in the Sicilian town of Augusta, designed in line with the former Italian seismic code, is considered as test structure. In particular, an r.c. framed structure with rectangular plan, composed of a basement and three storeys above ground level, is seismically isolated with a hybrid system including sixteen high-damping-rubber bearings (HDRBs) and twenty steel-PTFE low friction flat sliding bearings (LFSBs). An elevator shaft with steel framed structure crossing the isolation level is also placed in non symmetrical way along the longitudinal axis. A computer code for the nonlinear seismic analysis of base-isolated r.c. framed structures is improved by adding advanced nonlinear models of HDRBs and LFSBs. Finally, nonlinear dynamic analysis of the Augusta building is carried out with reference to near-fault earthquakes selected from the Pacific Earthquake Engineering Research center database and scaled in line with the design hypotheses adopted.

Peer-review under responsibility of the CINPAR 2018 organizers

Keywords: r.c. framed building; steel framed elevator shaft; hybrid base-isolation system; pounding effects; nonlinear dynamic analysis.

1. Introduction

Attention on the detrimental effects of near-fault earthquakes on reinforced concrete (r.c.) base-isolated structures has been growing in recent years. Long-duration and high-amplitude horizontal velocity pulses are expected at sites

* Corresponding author. Tel.: +39-0984-496908; fax: +39-0984-494045.
E-mail address: fabio.mazza@unical.it

Peer-review under responsibility of the CINPAR 2018 organizers
10.1016/j.prostr.2018.11.030

located near an active fault, producing notable displacement of the base-isolation system and amplification of inelastic demand in the superstructure (Mazza 2018). Recently, consideration has also been given to the effects of pounding of a seismically isolated building with the surrounding moat wall (Komodromos et al. 2007) and floor-to-floor (Agarwal et al. 2007; Polycarpou and Komodromos 2010) and floor-to-column (Pant and Wijeyewickrema 2012) seismic pounding of a base-isolated building with a fixed-base building. On the contrary, little research work has been done when the building has a basement and isolators are inserted at the top of the columns. However, the occurrence of pounding between closely spaced structural parts can be a serious hazard for base-isolated structures subjected to strong near-fault earthquakes, since seismic codes do not provide relevant specific provisions and practical considerations make the creation of a sufficiently wide gap problematic.

The aim of the present work is to investigate the occurrence of structural pounding in r.c. base-isolated framed structures with an insufficient gap between the elevator shaft and surrounding building (i.e. internal pounding on the building plan), focusing on the effects of near-fault earthquakes. Under these motions, the nonlinear response of elastomeric (e.g. high-damping-rubber bearings, HDRBs) and frictional (e.g. steel-PTFE low friction flat sliding bearings, LFSBs) bearings is expected to deviate from simplified viscoelastic and bilinear numerical models, respectively, proposed by seismic codes (Warn et al. 2007; Quaglini et al. 2014). The task here is to evaluate the effects of these advanced formulations of the base-isolation system on high horizontal displacements incompatible with design shear deformations of the HDRBs and internal seismic gap. To this end, a base-isolated commercial building, recently built in the Sicilian town of Augusta and designed in line with the former Italian seismic code (NTC 2008), is considered as test structure. Two structural solutions are examined, considering the base-isolated superstructure rigidly connected with a base-isolated elevator or separated from a fixed-base elevator by a gap. A computer code for the nonlinear seismic analysis of three-dimensional base-isolated r.c. framed structures (Mazza and Mazza, 2012) is improved by adding advanced nonlinear force-displacement laws of elastomeric and sliding bearings. Finally, nonlinear dynamic analysis of the building is carried out with reference to near-fault ground motions selected from the Pacific Earthquake Engineering Research center database (PEER 2014) and scaled in line with the design hypotheses adopted.

2. Nonlinear modelling of elastomeric and sliding bearings

Design procedures of base-isolation systems proposed by international seismic codes and guidelines generally allow for the use of simplified models to describe the hysteretic response of elastomeric and sliding bearings. A three-spring-three-dashpot viscoelastic linear model can be adopted for a HDRB, consisting of a linear elastic axial spring acting in parallel with a linear viscous dashpot both in the horizontal and vertical directions. Uncoupled elastic (i.e. $F_{K0,x}$, $F_{K0,y}$ and P_{K0}) and damping (i.e. $F_{C0,x}$, $F_{C0,y}$ and P_{C0}) axial forces proportional to horizontal and vertical displacement ($u_{H,x}$, $u_{H,y}$ and u_V) and velocity ($\dot{u}_{H,x}$, $\dot{u}_{H,y}$ and $\dot{u}_V$) are assumed

$$\begin{Bmatrix} F_x \\ F_y \end{Bmatrix} = \begin{Bmatrix} F_{K0,x} \\ F_{K0,y} \end{Bmatrix} + \begin{Bmatrix} F_{C0,x} \\ F_{C0,y} \end{Bmatrix} = K_{H0} \cdot \begin{Bmatrix} u_{H,x} \\ u_{H,y} \end{Bmatrix} + C_{H0} \cdot \begin{Bmatrix} \dot{u}_{H,x} \\ \dot{u}_{H,y} \end{Bmatrix} \cong K_{H0} \cdot \begin{Bmatrix} u_{H,x} \\ u_{H,y} \end{Bmatrix} + \left(\xi_H \cdot K_{H0} \cdot T_{1H} / \pi\right) \cdot \begin{Bmatrix} \dot{u}_{H,x} \\ \dot{u}_{H,y} \end{Bmatrix} \tag{1a,b}$$

$$P = P_{K0} + P_{C0} = K_{V0} \cdot u_V + C_{V0} \cdot \dot{u}_V \cong K_{V0} \cdot u_V + \left(\xi_V \cdot K_{V0} \cdot T_{1V} / \pi\right) \cdot \dot{u}_V \tag{1c}$$

where: K_{H0} and K_{V0} are the nominal values of the horizontal and vertical stiffness at the design displacement and zero axial load; ξ_H (ξ_V) and T_{1H} (T_{1V}) represent, respectively, the equivalent viscous damping ratio and fundamental vibration period in the horizontal (vertical) direction. Note that flexural and torsional rotations are neglected, on the assumption that top and bottom supports of the HDRBs do not experience significant rotation.

For constant values of the axial load (i.e. N=W, W being the weight of the superstructure) and friction coefficient (i.e. μ equal to the dynamic fast value μ_{max}), the force-displacement behaviour of a LFSB in the horizontal directions is idealized as bilinear (rigid-plastic) and represented by an hysteretic model with biaxial interaction

$$\begin{Bmatrix} F_x \\ F_y \end{Bmatrix} = \mu \cdot W \cdot \begin{Bmatrix} Z_x \\ Z_y \end{Bmatrix} = \mu_{max} \cdot W \cdot \begin{Bmatrix} Z_x \\ Z_y \end{Bmatrix} = \mu_{max} \cdot W \cdot \begin{Bmatrix} cos\theta \\ sin\theta \end{Bmatrix}, \quad \theta = \arctan\left(\frac{\dot{u}_{H,y}}{\dot{u}_{H,x}}\right) \tag{2a,b}$$

where the dimensionless quantities Z_x and Z_y are governed by two coupled differential equations which account for

the interaction between the x and y directions (Nagarajaiah et al. 1989). Furthermore, a gap element with infinitely rigid behaviour in compression is assumed in the vertical direction to consider the fact that a LFSB does not resist tensile axial loads and is thus free to uplift

$$P = N \;\text{ for } u_V \geq 0 \text{ and } P = 0 \;\text{ for } u_V < 0 \tag{2c}$$

where the equivalent viscous damping in the vertical direction is neglected.

Conversely, the use of a simple but reasonably accurate model is required to take into account the experimentally observed behaviour of the HDRBs during strong earthquakes (see Nagarajaiah and Ferrell 1999; Warn et al. 2007): i) high vertical forces significantly affect the horizontal response; ii) softening in the vertical direction occurs with notable lateral deformations; iii) horizontal stiffness lessens with increasing horizontal displacement. To this end, the three-spring-three-dashpot model can be modified assuming coupled nonlinear elastic springs in the horizontal and vertical directions, with a modified vertical displacement (u_V^*) taking into account the axial shortening or lengthening due to second order geometric effects

$$\begin{Bmatrix} F_x \\ F_y \end{Bmatrix} = \begin{Bmatrix} F_{K1,x} \\ F_{K1,y} \end{Bmatrix} + \begin{Bmatrix} F_{C0,x} \\ F_{C0,y} \end{Bmatrix} = K_{H0} \cdot \left(1 - \frac{P}{P'_{cr}} \right)^2 \cdot \left[1 - 0.325 \cdot tanh\left(\alpha \frac{\boldsymbol{u}_H}{t_r} \right) \right] \cdot \begin{Bmatrix} u_{H,x} \\ u_{H,y} \end{Bmatrix} + C_{H0} \cdot \begin{Bmatrix} \dot{u}_{H,x} \\ \dot{u}_{H,y} \end{Bmatrix} \tag{3a,b}$$

$$P = P_{K1} + P_{C0} = K_{V1} \cdot u_V^* + C_{V0} \cdot \dot{u}_V \cong \frac{K_{V0}}{1 + 48 \cdot \left(\frac{\boldsymbol{u}_H}{\pi \cdot D_b} \right)^2} \cdot sgn\left(u_V \right) \cdot \left(\left| u_V \right| - \frac{16 \cdot \alpha_b}{\pi^2 \cdot D_b \cdot S_2 \cdot \alpha_{K0}} \cdot \boldsymbol{u}_H^2 \right) + C_{V0} \cdot \dot{u}_V \tag{3c}$$

where: α is a dimensionless constant with a value of the total thickness of rubber (t_r); D_b is the diameter of the bearing; $\alpha_{K0}=K_{V0}/K_{H0}$ is the nominal stiffness ratio; $\alpha_b=h_b/t_r$, h_b being the total height of the bearing; $S_2=D_b/t_r$ is the secondary shape factor. It should be noted that $\mathbf{u}_H$ in Eqs. 3a-3b is expressed in mm. A reduced critical buckling load is introduced, with a bilinear approximation of the area-reduction method that takes into account the finite buckling capacity of a bearing at zero overlap area

$$P'_{cr} = 0.2 \cdot P_{cr} \text{ for } \frac{A_r}{A} \leq 0.2, \;\; P'_{cr} = P_{cr} \cdot \frac{A_r}{A} \;\text{ for } \frac{A_r}{A} > 0.2, \;\; P_{cr} = \frac{\pi \cdot G \cdot S_1 \cdot S_2 \cdot A}{2\sqrt{2}} \tag{3d}$$

where: G is the shear modulus of the rubber; $S_1=D_b/(4t_{r1})$ is the primary shape factor, t_{r1} being the thickness of the single layer of rubber; A is the bonded rubber area; A_r is the reduced area due to lateral displacement.

Similarly, experimental studies have uncovered the complex nonlinear behaviour of the LFSBs, highlighting the presence of numerous parameters affecting their friction coefficient at the sliding surface. Specifically, the dynamic friction coefficient monotonically increases with the sliding velocity up to a constant value (Constantinou et al. 1990). Moreover, the response of the LFSB shifts between sticking and sliding phases, at the breakaway and motion reversals, highlighting a static friction coefficient greater than the dynamic one (Quaglini et al. 2014). As a result, the force-displacement law of a LFSB in the horizontal direction can be improved by the following expression:

$$\begin{Bmatrix} F_x \\ F_y \end{Bmatrix} = \left[\mu_{max} - \left(\mu_{max} - \mu_{min} \right) \cdot e^{-\alpha_1 \cdot \dot{\boldsymbol{u}}_H} + \left(\mu_{st} - \mu_{min} \right) \cdot e^{-\alpha_2 \cdot \dot{\boldsymbol{u}}_H} \cdot \frac{\left| sgn\left(\dot{\boldsymbol{u}}_H \right) - sgn\left(\boldsymbol{u}_H \right) \right|}{2} \right] \cdot N \cdot \begin{Bmatrix} Z_x \\ Z_y \end{Bmatrix} \tag{4a,b}$$

where: μ_{min} and μ_{max} are the friction coefficients at low and fast sliding velocities, respectively; μ_{st} is the static friction coefficient when velocity is zero; α_1 is a parameter regulating the increase in dynamic friction with velocity; α_2 is a parameter regulating the transition from the static to the dynamic friction regime. Note that variation of the friction coefficient with axial pressure and temperature are neglected in the present study. Moreover, the axial load reported in Eqs. (4a,b) can be modified at any given moment during an earthquake in accordance with the following expression that also accounts for the vertical-horizontal coupling

$$N = W \cdot \left(1 + N_{OM} / W \right) \tag{4c}$$

where N_{OM} is the additional axial load, positive when compressive, due to the overturning moment produced by the horizontal ground acceleration.

3. Case study: the Augusta base-isolated building

A commercial building located in the Sicilian town of Augusta (Italy), designed in line with the previous Italian seismic code (NTC 2008), is considered as test structure (Fig. 1a). This r.c. framed structure with rectangular plan, composed of a basement and three storeys above the ground level, is seismically isolated with a hybrid system including sixteen HDRBs and sixteen LFSBs inserted at the top of rigid columns in the basement (Fig. 1b). A grid of rigid beams is also placed at the base of the superstructure on the isolation system.

(a) Picture of the building above the isolation level.

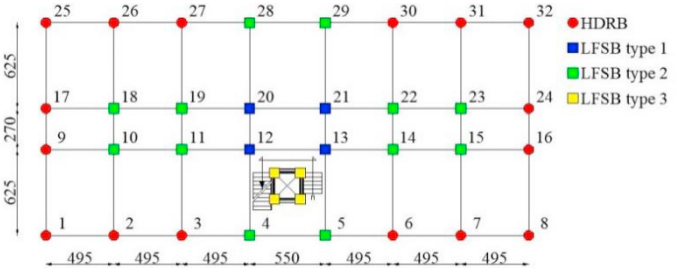

(b) Plan of the isolation level.

Fig. 1. Commercial building built in the Sicilian town of Augusta, Italy (units in cm).

The building plan is symmetrical with respect to the transversal, but not with respect to the longitudinal axis due to the presence of an eccentric elevator crossing the isolation level of the building, base-isolated with four LFSBs (Fig. 1b). The design of the seismically isolated structure is carried out on the basis of the following assumptions for the horizontal seismic loads at the ultimate life-safety (i.e. LS, in the design of the superstructure) and collapse prevention (i.e. CP, in the design of the base-isolation system) limit states: nearly elastic behaviour for the superstructure (behaviour factor, q=1.5); equivalent viscous damping of the isolation system ξ=15%; high-risk seismic zone (peak ground acceleration on rock, a_g=0.285g and 0.406g, at LS and CP limit states, respectively); stiff subsoil (class B, with subsoil parameter S_S=1.136 and 1.018 at the LS and CP limit states, respectively); topographic class T1 (stratigraphic parameter S_T=1); displacement demand of the base-isolation system at the CP limit state d_{dc}=272 mm. The gravity loads used in the design are represented by dead- and live loads, equal to: 6.47 kN/m^2 and 4 kN/m^2, for the first three levels; 5.27 kN/m^2 and 2 kN/m^2, for the roof level. Perimeter masonry infills without openings are placed along the short side of the building, at the second storey, and in the central bay of the long side of the building, at the first and second storey, while additional masonry infills are placed around the staircase. A cylindrical compressive strength of 30 N/mm^2 for the concrete and a yield strength of 450 N/mm^2 for the steel are assumed as characteristic values for the r.c. cross sections. The fundamental vibration period of the seismically-isolated structure is valued at T_{1H}=2.38 s, while the mass of the superstructure is equal to 2400 tons (Oliveto et al. 2013). The required horizontal stiffness for the isolation system is, therefore, 16.45 kN/mm, which is divided between the sixteen HDRBs on the hypothesis that the stiffness contribution of the LFSBs is negligible. In the commercial catalog provided by the manufacturer (FIP 2018) the isolator with the rounded up horizontal stiffness is type SI-N500/150. The LFSBs are characterized by a nominal diameter of 570 mm and a total height of 102 mm, of three types characterized by different values of the maximum loading capacity (i.e. type 1, VM 200/600/600, type 2, VM 150/600/600, and type 3, VM 25/600/600, shown in Fig. 1b).

The elevator shaft crosses the isolation plane and emerges in the basement, from where it is also accessible. The original design requires that the elevator shaft, constituted of a steel framed structure with double-T steel sections type HEA120, be rigidly connected to the superstructure at the landing levels and base-isolated with four LFSBs type 3 (Fig. 1b). An alternative structural configuration is that with the elevator shaft fixed-base and separated from the surrounding building by a gap. In this latter case, a seismic gap (g_d) along the in-plan principal directions, wide enough to avoid pounding, should be considered to accommodate displacement of the steel structure and deformation of the hybrid isolation system of the superstructure. More specifically, the elevator shaft is classified as non-dissipative (i.e. behaviour factor q=1) and designed at the CP limit state assuming g_d=360 mm in line with NTC08 provisions. Four different vertical positions of the elevator, corresponding to the basement and three floor

levels above it, are also considered along the building height. A total weight of 10 kN is assumed for the elevator, including a dead load of 5 kN plus a live load of 5 kN corresponding to the maximum number of persons allowed.

To establish whether the design gap g_d (Fig. 2a) is large enough to address sizeable horizontal displacements induced by NF ground motions, the relative displacements between structurally independent units of the Augusta building require monitoring. In particular, horizontal displacements of the fixed-base elevator shaft (Es) and base-isolated surrounding building (Sb) shown in Fig. 1b, along the in-plan X (i.e. $u_{Es,i}$ and $u_{Sb,i}$) and Y (i.e. $v_{Es,i}$ and $v_{Sb,i}$) directions, are evaluated

$$g_{X,i}(t) = g_d + u_{Es,i}(t) - u_{Sb,i}(t), \quad g_{Y,i}(t) = g_d + v_{Es,i}(t) - v_{Sb,i}(t), \quad i=1\text{-}4 \tag{5a,b}$$

considering all four couples of corner joints to take account of torsional effects resulting from unsymmetrical layout of the elevator (Fig. 2b). It should be noted that the design gap (g_d) is assumed with positive values when the coordinate of the Es corner is greater than that of the corresponding Sb corner.

(a) Undeformed configuration. (b) Deformed configuration.

Fig. 2. Pounding effects between the fixed-base elevator shaft and base-isolated surrounding building.

4. Numerical results

With a view to studying the effects of nonlinear modelling of the isolation system on the dynamic analysis of r.c. framed buildings subjected to near-fault earthquakes (EQs) containing long-period horizontal velocity pulses, the simplified (SM) and advanced (AM) three-degree-of-freedom models of HDRBs and LFSBs previously described in Section 3 are implemented through a computer code proposed in a previous work (Mazza and Mazza 2012). R.c. frame members of the superstructure are described by a lumped plasticity model, with hardening ratio equal to 3%, in which the axial load and biaxial bending moment interaction of the r.c. cross-sections is computed by a piecewise linearization of the limit surface. On the other hand, an elastic-linear response consistent with the design hypotheses is adopted for the steel framed structure of the elevator shaft, in both the base-isolated and fixed-base configurations. In the Rayleigh hypothesis, the damping matrices of the r.c. and steel framed structures are assumed as a linear combination of the mass and stiffness matrices, assuming a viscous damping ratio equal to 2% with reference to the two vibration periods corresponding to high-participation modes with components prevailing in the horizontal directions. Incremental dynamic analysis (IDA) of the Augusta building is carried out through a series of nonlinear dynamic tests under near-fault ground motions selected motions from the Pacific Earthquake Engineering Research center database (PEER 2014) and scaled to a submultiple (a_g) of the corresponding PGA value. It should be noted that the pulse-like characteristic of the NF motions may be altered with the scaling (Mazza 2018), so results of the nonlinear dynamic analysis will be presented both in terms of mean and maximum values separately obtained for each ground motion.

Firstly, to represent seismic effects in the HDRBs of the isolation system of the Augusta building, mean and maximum values of shear strain resulting from seismic displacement (γ_s) and total shear strain (γ_{tot}), also including shear contributions due to axial compression (γ_c) and angular rotation (γ_a), are plotted in Figs. 3a and 3b, respectively. In particular, simplified (SM) and advanced (AM) force-displacement laws for predicting the highly nonlinear behaviour of elastomeric and sliding bearings are compared for increasing values of the dimensionless

acceleration ratio α_a (=a_g/g), until reaching value α_a=1 corresponding to the CP limit state. As shown, the AMs representing the HDRBs and LFSBs are the most conservative, producing upper-bound mean and maximum values. Moreover, these maximum values of γ_s and γ_{tot} have widely exceeded the corresponding thresholds imposed by NTC08 (i.e. γ_s=2 and γ_{tot}=5) for α_a>0.75 and α_a>0.9, respectively. The distribution of local damage in the r.c. frame members at the CP limit state is presented in Figs. 3c,d with regard to the height of the superstructure, considering the same final value of the dimensionless acceleration (i.e. α_a=1) for each ground motion. Mean and maximum values of the curvature ductility demand of beams (Fig. 3c) and columns (Fig. 3d) are compared with the corresponding ultimate values. As can be observed, low values of the mean ductility demand are obtained for all frame members as a result of a significant overstrengthening, partly due to the assumption on the nominal value of the behaviour factor. Moreover, the ductility demand of the columns is higher than that observed for the beams, with an amplification of the maximum values at the first level where the NTC08 threshold is exceeded *slightly* (Fig. 3d). Note that the three-degree-of-freedom simplified models of the HDRBs and LFSBs are found be more conservative than the advanced ones, producing upper bound values of ductility demand.

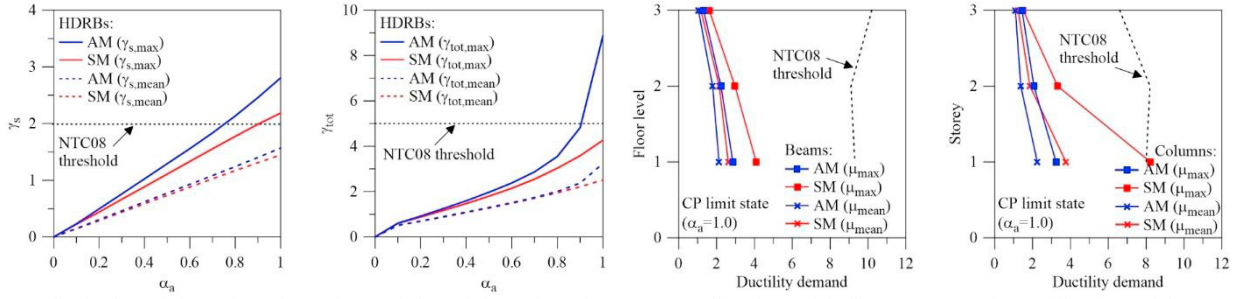

(a) Seismic shear deformation of the HDRBs. (b) Total shear deformation of the HDRBs. (c) Ductility demand for beams of the superstructure. (d) Ductility demand for columns of the superstructure.

Fig. 3. Mean and maximum response parameters at CP limit state.

Afterwards, a parametric investigation is carried out on the minimum relative distance necessary in order to avoid internal pounding along the height of the Augusta building, with a focus on the structural configuration in which the steel elevator shaft is fixed-base in the basement while the surrounding r.c. structure is seismically-isolated at ground level. To this end, maximum values of the relative displacements are calculated at the CP limit state for the four couples of corner joints depicted in Fig. 2 (i.e. g_i, i=1-4), along the in-plan X (Fig. 4) and Y (Fig. 5) principal directions. Size gap imposed by NTC08 (i.e. g_d) is also represented with a dashed line, under the assumption that the same value is assumed around the elevator shaft. Specifically, four cases are compared considering that the mass of the elevator is added to the basement (Figs. 4a and 5a) and ground (Figs. 4b and 5b), first (Figs. 4c and 5c) and second (Figs. 4d and 5d) levels of the Augusta building. As shown, the occurrence of internal pounding is confirmed at all levels of the superstructure in the case of near-fault seismic input, especially in the X direction (Fig. 4), with the only exception being the ground level (i.e. floor level zero in Figs. 4a and 5a).

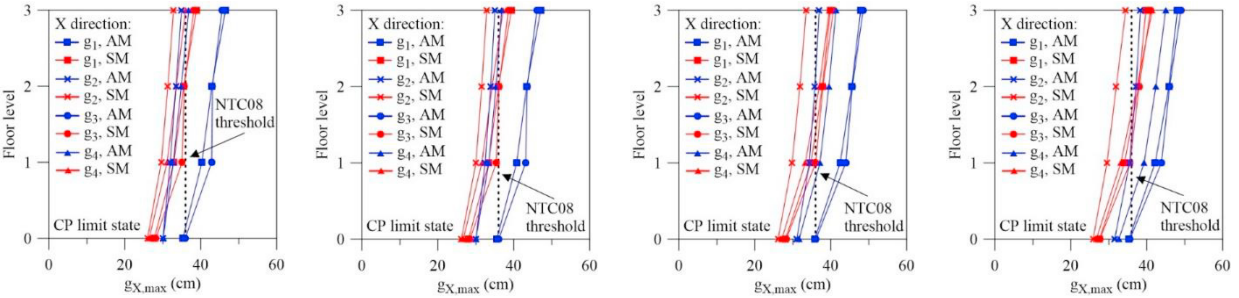

(a) Elevator at basement. (b) Elevator at ground level. (c) Elevator at first level. (d) Elevator at second level.

Fig. 4. Maximum relative displacement between the elevator shaft and surrounding building at CP limit state (X direction).

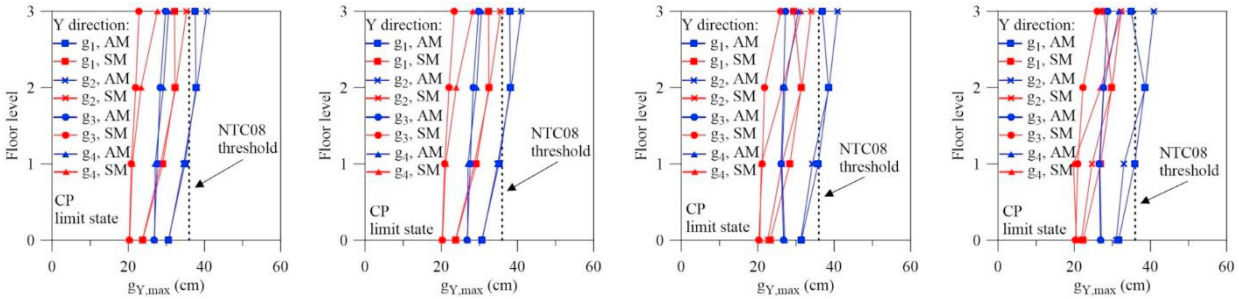

(a) Elevator at basement. (b) Elevator at ground level. (c) Elevator at first level. (d) Elevator at second level.

Fig. 5. Maximum relative displacement between the elevator shaft and surrounding building at CP limit state (Y direction).

Noticeable torsional effects are induced by the eccentric position of the elevator shaft in the building plan and the influence of the position of the additional elevator mass along the building height is also observed, with increasing values of the relative displacement as the elevator moves upwards. It is interesting to note that the size gap is sensitive to nonlinear modelling assumptions of the isolation system, with the greatest values of the maximum relative displacement when the advanced models of HDRBs and LFSBs are considered.

Finally, time histories of the relative displacement between the elevator shaft and surrounding building subjected to the horizontal components of the Chi-Chi earthquake are plotted in Fig. 6 for the acceleration ratio α_a=1.0. More specifically, curves concerning the four couples of corner joints at the ground (zero level) and roof (third level) of the superstructure are compared when the simplified and advanced numerical models of HDRBs and LFSBs are taken into account. The highest values of the relative displacement are reported in Fig. 6, where only results for the X direction and elevator positioned at the second level are represented. It should be noted that, in accordance with the positive sign convention of the seismic gap reported in Fig. 2a, only negative (i.e. the Es1-Bs1 and Es3-Bs3 couples of corner joints) and positive (i.e. the Es2-Bs2 and Es4-Bs4 couples of corner joints) values of the NTC08 threshold are reported in Figs. 6a,c and Figs. 6b,d, respectively. As shown, NTC08 seismic gap is sufficient to allow relative displacements at ground level without internal pounding also when the elevator stops at the second level, while the roof level is confirmed as the most vulnerable to pounding effects, exceeding the NTC8 threshold for both simplified and advanced modelling assumptions of the isolation system.

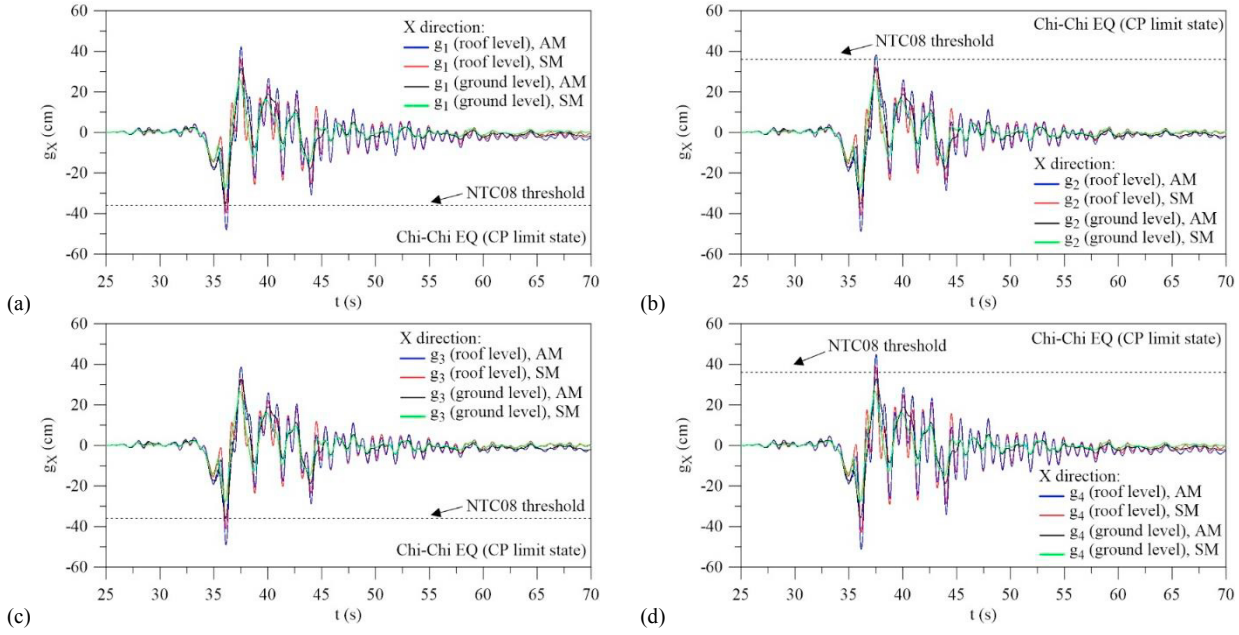

Fig. 6. Time-histories of the relative displacement between the elevator shaft and surrounding building at CP limit state (X direction).

5. Conclusions

The effects of pulse-type near-fault earthquakes on the nonlinear dynamic response of an r.c. framed structure, seismically isolated with a hybrid system at the ground level and crossed by the steel framed structure of an elevator shaft, are investigated with a view to evaluating the importance of simplified and advanced nonlinear modelling of HDRBs and LFSBs. Different cases are examined combining four vertical positions of the elevator cabin (i.e. the basement and three floors above it) with two structural configurations of the elevator shaft (i.e. base-isolated and rigidly connected to the superstructure or fixed-base and separated from it by a gap). The numerical results indicate that the advanced models of the isolation system are the most conservative when evaluating mean and maximum values of response parameters for the elastomeric bearings, while the simplified models may be adopted for a precautionary seismic assessment of the superstructure. Despite the presence of a design seismic gap, the occurrence of internal pounding is highlighted at all levels of the superstructure in the case of a fixed-base elevator, with the only exception being at ground level. These unexpected structural impacts are mainly due to deformations of both adjacent structures that can be amplified in a near-fault area, even though the gap is created in such a way as to take into consideration not only the design displacement of the isolation system at CP limit state but also the maximum horizontal displacement of the fixed base elevator. Additional pounding depends on torsional effects induced by the eccentric position of the elevator shaft in the building plan, with increasing values of the relative horizontal displacement as the additional mass of the elevator moves upwards.

Acknowledgements

This work was financed by Re.L.U.I.S. (Italian network of university laboratories of earthquake engineering), in line with “Convenzione D.P.C.–Re.L.U.I.S. 2018, PR6 line, Isolation and Dissipation”.

References

Agarwal, V.K., Niedzwecki, J.M., van de Lindt, J.W., 2007. Earthquake induced pounding in friction varying base isolated buildings. Engineering Structures 29, 2825–2832.

Constantinou, M.C., Mokha, A. and Reinhorn, A.M., 1990. Teflon bearings in base isolation. II: modeling. Journal of Structural Engineering 116(2), 455-474.

FIP Industriale S.p.A., 2018. Elastomeric isolators -Series SI. https://www.fipindustriale.it/index.php?area=106&menu=67&page=167.

Gesualdi, G., Cardone, D., Rosa, G., 2018. Finite element model updating of base-isolated buildings using experimental results of in-situ tests. Soil Dynamics and Earthquake Engineering 10.1016/j.soildyn.2018.02.003

Komodromos, P., Polycarpou, P., Papaloizou, L., Phocas, M.C., 2007. Response of seismically isolated buildings considering poundings. Earthquake Engineering and Structural Dynamics 36, 1605–1622.

Mazza, F., 2018. Seismic demand of base-isolated irregular structures subjected to pulse-type earthquakes. Soil Dynamics and Earthquake Engineering 108, 111-129.

Mazza, F., Mazza, M., 2012. Nonlinear modeling and analysis of r.c. framed buildings located in a near-fault area. The Open Construction & Building Technology Journal 6, 346-354.

Nagarajaiah, S., Reinhorn, A.M., Constantinou, M.C., 1989. Nonlinear dynamic analysis of three-dimensional base isolated structures (3D-basis). National Center for Earthquake Engineering Research, State University of New York, Buffalo, Technical Report NCEER-89-0019.

Nagarajaiah, S., Ferrell, K., 1999. Stability of elastomeric seismic isolation bearings. Journal of Structural Engineering 125(9), 946-954.

NTC 2008. Technical Regulations for the Constructions. Italian Ministry of the Infrastructures, D.M. 14-01-2008 and C.M. 2-2-2009.

Oliveto, G., Athanasiou, A., Granata, M., 2013. Blind simulation of full scale free vibration tests on a three story base isolated building. Proceedings of the 10th International Conference on Urban Earthquake Engineering, Tokyo, Japan, March 1-2.

Pant, D.R., Wijeyewickrem, A.C., 2012. Structural performance of a base-isolated reinforced concrete building subjected to seismic pounding. Earthquake Engineering & Structural Dynamics 41(12), 1709-1716.

PEER, 2014. Pacific Earthquake Engineering Research Center database. http://ngawest2.berkeley.edu.

Polycarpou, P.C., Komodromos, P., 2010. On poundings of a seismically isolated building with adjacent structures during strong earthquakes. Earthquake Engineering & Structural Dynamics 39, 933-940.

Quaglini, V., Bocciarelli, M., Gandelli, E., Dubini, P., 2014. Numerical assessment of frictional heating in sliding bearings for seismic isolation. Journal of Earthquake Engineering 18, 198-216.

Warn, G.P., Whittaker, A.S., Constantinou, M.C., 2007. Vertical stiffness of elastomeric and lead–rubber seismic isolation bearings. Journal of Structural Engineering 133, 1227-1236.